Optics Letters

High-frequency vector harmonic mode locking driven by acoustic resonances

H. J. Kbashi,[1] S. V. Sergeyev,[1,*] M. Al-Araimi,[1] A. Rozhin,[1] D. Korobko,[2] and A. Fotiadi[2,3]

[1]School of Engineering and Applied Science, Aston University, Aston Triangle, Birmingham, B4 7ET, UK
[2]Ulyanovsk State University, 42 Leo Tolstoy Street, Ulyanovsk, 432970, Russian Federation
[3]Université de Mons, Faculté Polytechnique, Boulevard Dolez 31, 7000 Mons, Belgium
*Corresponding author: s.sergeyev@aston.ac.uk

Received 2 August 2019; revised 14 September 2019; accepted 18 September 2019; posted 19 September 2019 (Doc. ID 374487); published 17 October 2019

A controllable passive harmonic mode locking (HML) in an erbium-doped fiber laser with a soliton pulse shaping using a single-wall carbon nanotube has been experimentally demonstrated. By increasing the pump power and adjusting the in-cavity polarization controller, we reached the 51st-order harmonic (902 MHz) having the output power of 37 mW. We attribute the observed high-frequency HML to the electrostriction effect caused by periodic pulses and leading to excitation of the radial and torsional-radial acoustic modes in the transverse section of the laser. The exited acoustic modes play the role of the bandpass filter, which stabilizes the high-frequency HML regime.

https://doi.org/10.1364/OL.44.005112

High repetition rate, passively mode-locked fiber lasers based on carbon nanotubes are excellent platforms for ultrafast pulse generation with advantages including good beam quality, alignment-free operation, efficient heat dissipation, pumping efficiency, power scalability, and simple operation configuration. These advantages have unlocked a number of applications, including material processing, optical communications, metrology, and biomedicine [1–5]. Typically, most of the fiber lasers operate at a repetition rate of tens of megahertz due to the relatively long laser cavity of tens of meters. However, particular applications such as telecommunication, spectroscopy, and metrology require higher repetition rates of hundreds of megahertz. The harmonic mode locking (HML) is a practical pathway to increase the repetition rate 100 times through selective excitation of the harmonic of the fundamental frequency [6–12]. The HML is based on the multi-pulsing that emerges as a result of the interplay between the laser cavities' bandwidth constraints and the energy quantization for mode-locked pulses [13]. The growth of the mode-locked spectral bandwidth with increased pump power is limited by the gain bandwidth of the cavity. To overcome this constraint, a single pulse is split into many pulses with energy shared between the pulses and bandwidths within the gain bandwidth window. The splitting is accompanied with the electrostriction effect in the form of excitation of the radial $R_{0\,m}$ and torsional-radial $TR_{2\,m}$ acoustic modes. The acoustic effect through $R_{0\,m}$ mode excitation results in the fiber core refractive modulation and, thus, enables HML stabilization at frequencies lower than ~500 MHz [7]. For higher repetitive rates above 500 MHz, torsional-radial $TR_{2\,m}$ acoustic modes can be excited with a spectrum expanded over 1 GHz [7,14]. Unlike $R_{0\,m}$ modes, the $TR_{2\,m}$ modes do not perturb the fiber core refractive index significantly but only affect the fiber birefringence. The excitation efficiency for $TR_{2\,m}$ modes is maximal for linearly polarized pulses and zero for circularly polarized pulses [14,15]. Acoustically induced fluctuations of the fiber birefringence are rather small and comparable with the random linear birefringence of a single-mode fiber. Therefore, they have never been considered as a candidate for laser stabilization mechanism. Therefore, a challenging task still exists in the context of revealing the role of the polarization-dependent torsional-radial $TR_{2\,m}$ acoustic modes in the stabilization of HML.

In this Letter, for unidirectional erbium-doped fiber laser mode-locked by carbon nanotubes, we demonstrate the control of the repetition rates from fundamental (17.67 MHz) experimentally to the 51st (902 MHz) based on adjustment of the pump power and in-cavity polarization controller for tuning the intra-cavity birefringence. We have found that the presence of the elliptical state of polarization (SOP) for the frequencies exceeding 500 MHz is supporting evidence of excitation of $TR_{2\,m}$ mode.

The configuration of the scalable HML fiber laser setup is illustrated in Fig. 1(a). This setup consists of single-mode all-fiber integrated components for an alignment-free and compact system. The fiber ring cavity is composed of a 0.75 m long erbium-doped active fiber (*Liekki Er80-8/125* group velocity dispersion (GVD) of −20 ps^2/km at 1550 nm) and a single-mode (SM) fiber with GVD of −22.8 ps^2/km at 1550 nm), which is pumped by fiber-pigtailed 980 nm pump laser diode via a 980/1550 WDM. The overall cavity length is 17 m. In addition, the set-up includes a polarization-independent optical isolator to ensure unidirectional propagation and a single polarization controller inside the cavity to continuous controlling of the net cavity birefringence. A 70:30 fused fiber output coupler is used to redirect out of the cavity of 30% of the signal power to the spectral and temporal diagnostics devices.

The laser output radiation from the 30% coupler is detected using a 50 GHz fast photodetector (Finisar XPDV2320R) with 33 GHz bandwidth. The output is recorded by an 80 GSa/s sampling rate oscilloscope (Agilent DSOX93204A). The radio-frequency (RF) spectrum and the optical spectrum (OS) have been recorded by using RF spectrum analyzer (Rohde and Schwarz, 10 Hz-13.6 GHz) and the OS analyzer (ANDO AQ6317B), and the pulse width–with the help of the auto-correlator (Pulsecheck). The resolution used in the RF and OS measurements is 3 Hz and 0.02 nm, respectively. To get insight into the polarization laser dynamics at the slow time scales of 1 μs–20 ms (averaging over 56 round trips), we used a polarimeter (IPM5300, Thorlabs) to record the normalized Stokes parameters s_1, s_2, and s_3. These are related to the output powers of two linearly cross-polarized SOPs, I_x and I_y, and to the phase difference between them $\Delta\phi$ [13–15]:

$$S_0 = I_x + I_y, \quad S_1 = I_x - I_y, \quad S_2 = 2\sqrt{I_x I_y}\cos\phi,$$
$$S_3 = 2\sqrt{I_x I_y}\sin\phi, \quad s_i = \frac{S_i}{\sqrt{S_1^2 + S_2^2 + S_3^2}}, \quad (i = 1, 2, 3). \tag{1}$$

The single-wall carbon nanotube (SWCNT) SA used in this experiment is a high-purity, high-metallic content (CG200) SWCNT-PVA composite. Before the experiment, 0.2 mg/mL of CG200 were placed in deionized water with 2% sodium dodecylbenzenesulfonate surfactant; the solution is sonication for 1 h at 130 W and 20 kHz. Large bundles and impurities were removed using ultracentrifugation. The resulting solution was mixed with polyvinyl alcohol (PVA) powder and placed in the Petri dish to form the SWCNT-PVA film. The saturation power and modulation depth of the SWCNT-PVA film were 3 MW/cm^2 and 5%, respectively.

Due to the SWCNT SA, self-started mode locking [Fig. 1(b)] can be easily achieved as soon as the lasing threshold (18 mW) is reached with the fundamental pulse repetition rate of 56.6 ns (17.67 MHz). The OS of the mode-locking laser pulses [Fig. 1(c)] exhibits the shape typical for the soliton operation regime with clear distinct Kelly sidebands in the spectrum. The main components of the spectrum are in wavelengths near 1563.6nm, with a 3 dB spectral bandwidth as 2.85 nm. The pulse duration shown in Fig. 1(d) is about 990 fs, and it is fitted to the hyperbolic secant pulse profile. Correspondingly, the time-bandwidth product is 0.3481, indicating that the output pulse is almost transform limited.

The fiber laser starts to emit HML pulses directly by increasing the pump power slightly higher than the laser threshold to about 23 mW with an appropriate setting of the intra-cavity polarization controller (PC1). Figure 2 shows the oscilloscope traces of the typical mode-locked and HML operation evaluation at different pump power. We found that the characteristic of the HML in our fiber lasers is that the pulse repetition rate increases with the increase of pump power and adjusting the PC1.

For example, with proper adjustment of both PC1 and PC2, the first and second HML could be achieved at a pump power of 27 and 29 mW, respectively. Then multiple pulses from 3rd toward up to the 51st are generated within the laser round trip, as shown in Figs. 2(b)–2(e) with further increasing of the pump power and adjustment of PC1. For pump power of 32 mW we observed multi-pulsing which is transformed to HML for increased pump power as follows: 14th harmonic (247. 38 MHz) for 63 mW, 42nd harmonic (742.14 MHz) for 138 mW and 51st harmonic (902 MHz) for 180 mW [Figs. 2(c)–2(e)].

The RF spectra for the sequence of ML and different HML regimes at different pump powers are shown in Fig. 3. The RF spectrum at the fundamental frequency $f_1 = 17.67$ MHz at 23 mW [Fig. 3(a), peak 1] has a peak-to-pedestal ratio of ~80 dB. The additional peaks (peak 2) with a spectral power of 30 dB or lower emerge at 63 mW at different frequencies. These peaks moved towards their centers of mass located at the distance of $f_1/2$ from the main peak with increased pump power and adjustment of the PC1. As shown in our recent publications, such peaks are caused by vector resonance multimode instability (VRMI) [16,17]. In the case of VRMI, adjustment of the in-cavity polarization controller leads to the spatial modulation of the SOP of the in-cavity lasing field with spatial frequency proportional to the birefringence strength. As a result, the dispersion relation leads to the emergence of the additional satellite lines in the RF spectrum with the frequency splitting proportional to the birefringence strength [16,17]. We found that it is very hard to match the two neighboring polarization satellites as it reaches to a limit space and the repulsive far from each other. In addition, the matching of the

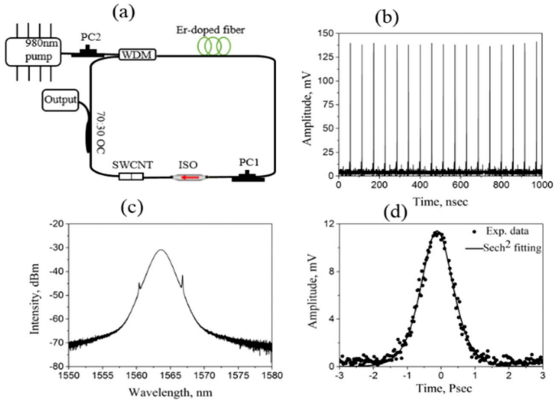

Fig. 1. (a) Harmonic mode-locked fiber laser experimental cavity and (b) mode-locked oscilloscope traces at 23 mW; (c) OS and (d) corresponding pulse duration.

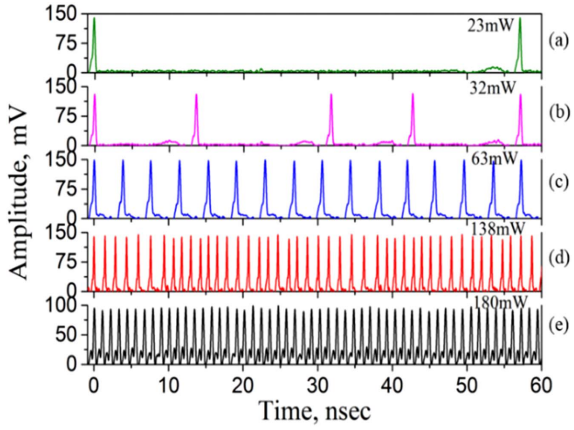

Fig. 2. Oscilloscope trace of the output pulses at different pump powers: (a) 23, (b) 32, (c) 63, (d) 138, and (e) 180 mW.

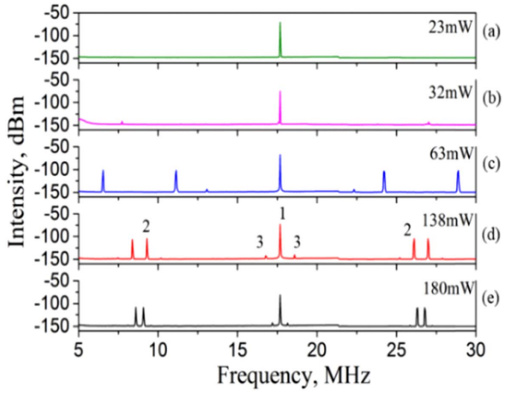

Fig. 3. RF spectrum of the output pulses at different pump powers: (a) 23, (b) 32, (c) 63, (d) 138, and (e) 180 mW.

polarization satellites with the fundamental frequency or even near to it leads the laser back to emit normal mode-locking regimes. However, the RF peak-to-pedestal ratio of the 51st harmonic is about of 68 dB, as shown in Fig. 4. The linewidth of this harmonic laser line is 50 KHz.

The optical spectra of the HML regimes are illustrated in Fig. 5. The OS was centered at about 1564 nm at low pump power [Figs. 5(a)–5(c)] and then shifted towards 1562 at higher pump power [Figs. 5(d) and 5(e)]. In addition, the spectrum at the pump power of 63 mW (Fig. 5) demonstrates a strong CW component which can emerge as the result of the polarization

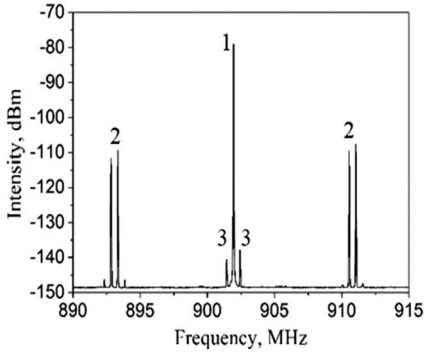

Fig. 4. RF spectrum of the 51st harmonic mode-locked pulses.

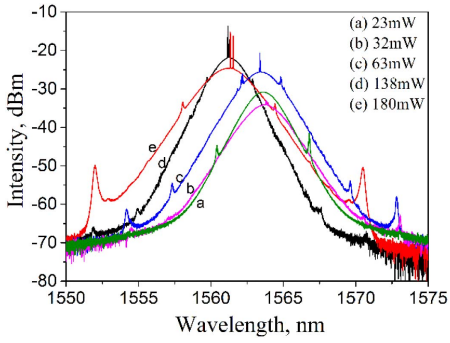

Fig. 5. Optical spectra of the HML at different pump powers: (a) 23, (b) 32, (c) 63, (d) 138, and (e) 180 mW.

and pump power satellites, as explained in Fig. 3(c). The CW component increased as two CW lines appeared at increasing the pump power to 138 mW [Fig. 5(d)]. These two CW components became closer [Fig. 5(e)] to each other, just as the two neighboring polarization satellites in Fig. 3(e). In addition, Fig. 5 shows a large number of the sidebands in the OS.

Figure 6(a) shows the pulse repetition rate that was measured for the output pulses. The pulse repetition rate changes almost linearly from 17.67 to 902 MHz, together with the harmonic order. The pumping efficiency was estimated as ~5.44 MHz mW^{-1}. Figure 6(b) shows the average output power and pulse energy that were measured. The maximum average power was 37.2 mW at a maximum pump power of 180 mW. The pulse energies of the output pulses were in the range of 38 to 97 pJ.

To evaluate the $R_{0\,m}$ and $TR_{2\,m}$ acoustic mode contribution to the stabilization of the HML operation, we use data recorded by a polarimeter. The polarization dynamics for the HML regimes are shown in Fig. 7. The Stokes parameters at the Poincaré sphere shown in Fig. 7(a) are related to the polarization attractor at the Poincaré sphere in the form of a fixed point for all of the generated HML regimes. If the degree of polarization (DOP) is close to 100%, then the fixed point at the

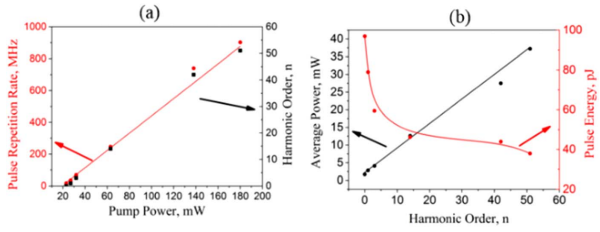

Fig. 6. (a) Pulse repetition rate and the harmonic order of the output pulses as a function of the pump power. (b) Average output power and harmonic pulse energy as a function of the harmonic order (n).

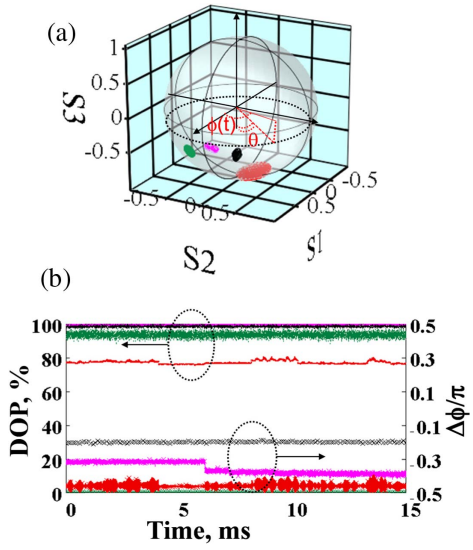

Fig. 7. (a) SOPs; (b) DOP and the phase difference $\Delta\phi$ for different pump powers: 23 (green), 32 (cyan), 138 (red), and 180 mW (black).

Poincaré sphere indicates a stable operation for all HML. For 23 mW pump power [green lines in Figs. 7(a) and 7(b)], the position of the attractor close to the south pole of the Poincaré sphere, DOP ≈ 100%, and the phase difference of $\Delta\phi \approx -0.5\pi$ are related to the stable left circularly polarized SOP. As follows from Figs. 2 and 6, the low pulse power is below the threshold of HML excitation. For the pump power at 32 mW, the attractor is slightly shifted to the elliptically polarized SOP with the $\Delta\phi \approx -0.35\pi$, DOP ≈ 100% and, as follows from Fig. 2, the dynamics takes the form of the unstable multi-pulsing. For the pump power of 138 mW, $\Delta\phi \approx -0.5\pi$, DOP ≈ 78%, which means that the real polarization attractor has a different form. To reveal this form, we present dynamics in the form of a circle at the Poincaré sphere, as shown in Fig. 7(a), i.e., $S_1 = S_0\cos(\phi(t))\sin(\theta)$, $S_2 = S_0\sin(\phi(t))\sin(\theta)$, and $S_3 = S_0\cos(\theta)$. As a result of averaging over 56 round trips, $S_1 = S_2 \approx 0$, $S_3 \approx S_0\cos(\theta)$, $s_3 = 1$ or $s_3 = -1$ (for $\pi/2 < \theta < \pi$), and DOP ≈ $|\cos(\theta)| = 0.8$ and thus the averaged SOP is close to the circularly polarized SOP, unlike the real dynamically evolving elliptically polarized SOP. Such a case can justify the existence of the dynamically evolving elliptically polarized in-cavity field that can excite the $TR_{2\,m}$ acoustic mode with the frequency of 742.14 MHz, which is beyond the spectrum of $R_{0\,m}$ modes [14]. In the case of 180 mW pump power, $\Delta\phi \approx -0.2\pi$, and DOP ≈ 100%; thus, the in-cavity field is elliptically polarized. As a result, the $TR_{2\,m}$ acoustic mode with the frequency of 902 MHz can be excited.

In conclusion, we demonstrated a high HML in SWCNT SA erbium-doped fiber laser using the acoustic-optic effect. Under different launched pump powers and appropriate adjustments of the birefringence strength in the cavity, controllable HML from the first up to the 51st order has been obtained. In addition, we have found that the 42nd and 51st HML regimes, corresponding to the repetition rates of 742.14 and 902 MHz, are beyond the spectrum of $R_{0\,m}$ acoustic modes. Given that the state of polarization of the lasing field is an elliptical for both cases, we conclude that these HML regimes can be enabled by $TR_{2\,m}$ acoustic modes having the spectrum beyond 1 GHz [14]. The stability of HML has been shown in terms of the SNR level as large as 68 dB which means the laser emits high-quality pulses with low-energy fluctuations. Unlike HML stabilization based on $R_{0\,m}$ modes, theoretical characterization of the $TR_{2\,m}$-based HML stabilization requires strong coupling between orthogonal linear-polarized modes [14]. For the erbium-doped mode-locked fiber laser, such coupling has been specified in our previous publications based on the model that goes beyond the limitations of the previously used models based on either coupled nonlinear Schrödinger or Ginzburg–Landau equations [16–18]. The model accounts for the dipole mechanism of the light absorption and emission, and light-induced anisotropy caused by polarized pump field [16–18].

Funding. Leverhulme Trust (RPG-2014-304, VP2-2016-042); Russian Science Foundation (18-12-00457).

REFERENCES

1. T. Udem, R. Holzwarth, and T. W. Hansch, Nature **416**, 233 (2002).
2. T. M. Fortier, M. S. Kirchner, F. Quinlan, J. Taylor, J. Bergquist, T. Rosenband, N. Lemke, A. Ludlow, Y. Jiang, C. W. Oates, and S. A. Diddams, Nat. Photonics **5**, 425 (2011).
3. D. Solli, C. Ropers, P. Koonath, and B. Jalali, Nature **450**, 1054 (2007).
4. J. Mandon, G. Guelachvili, and N. Picque, Nat. Photonics **3**, 99 (2009).
5. P. Grelu and N. Akhmediev, Nat. Photonics **6**, 84 (2012).
6. A. B. Grudinin and S. Gray, J. Opt. Soc. Am. B **14**, 144 (1997).
7. A. I. Trikshev, V. A. Kamynin, V. B. Tsvetkov, and P. A. E. Itrin, Quant. Electron. **48**, 1109 (2018).
8. F. Amrani, A. Haboucha, M. Salhi, H. Leblond, A. Komarov, and P. Grelu, Opt. Lett. **34**, 2120 (2009).
9. H.-R. Chen, K.-H. Lin, C.-Y. Tsai, H.-H. Wu, C.-H. Chen, and W.-F. Hsieh, Opt. Lett. **38**, 845 (2013).
10. X. Li, W. Zou, and J. Chen, Opt. Express **23**, 21424 (2015).
11. C. S. Jun, S. Y. Choi, F. Rotermund, B. Y. Kim, and D.-I. Yeom, Opt. Lett. **37**, 1862 (2012).
12. T. Habruseva, C. Mou, A. Rozhin, and S. V. Sergeyev, Opt. Express **22**, 15211 (2014).
13. F. Li, P. K. A. Wai, and J. N. Kutz, J. Opt. Soc. Am. B **27**, 2068 (2010).
14. R. M. Shelby, M. D. Levenson, and P. W. Bayer, Phys. Rev. B **31**, 5244 (1985).
15. A. N. Pilipetskii, A. V. Luchnikov, and A. M. Prokhorov, Sov. Lightwave Commun. **3**, 29 (1993).
16. S. V. Sergeyev, H. Kbashi, N. Tarasov, Y. Loiko, and S. A. Kolpakov, Phys. Rev. Lett. **118**, 033904 (2017).
17. S. V. Sergeyev, H. Kbashi, C. Mou, A. Martinez, and S. Kolpakov, V. Kalashnikov, *Nonlinear Guided Wave Optics: a Testbed for Extreme Waves* (IOP Publishing, 2018), Chap. 9, p. 9–01.
18. S. V. Sergeyev, Phil. Trans. R. Soc. A **372**, 20140006 (2014).